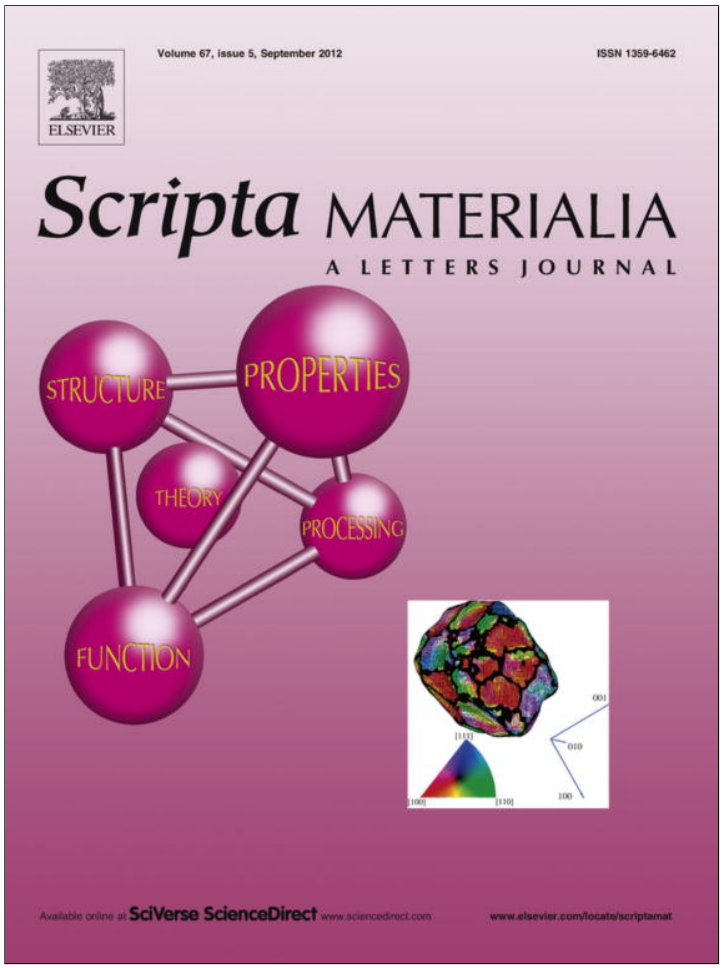

Available online at www.sciencedirect.com

SciVerse ScienceDirect

Scripta Materialia 67 (2012) 507–510

Scripta MATERIALIA

www.elsevier.com/locate/scriptamat

Metal ion implantation of multiwalled boron nitride nanotubes

E.A. Obraztsova,[a] D.V. Shtansky,[a,*] A.N. Sheveyko,[a] M. Yamaguchi,[b] A.M. Kovalskii[a] and D. Golberg[b,*]

[a] *National University of Science and Technology "MISIS", Leninskii prospect 4, Moscow 119049, Russia*
[b] *National Institute for Materials Science (NIMS), Namiki 1-1, Tsukuba, Ibaraki 3050044, Japan*

Received 29 May 2012; accepted 11 June 2012
Available online 16 June 2012

Recent progress in boron nitride nanotube (BNNT) synthesis has opened new possibilities for utilization of the attractive combination of the excellent mechanical characteristics and superb thermal and chemical stabilities of BNNTs for the creation of new structural and functional reinforced materials. In this work we have applied metal ion implantation to prepare novel BNNT/metal matrix composites. The resulting structures have been thoroughly studied by high-resolution transmission electron microscopy and Raman spectroscopy.

Keywords: Boron nitride nanotubes; Nanotubes/metal composites; Ion implantation; Structure

Most of the structural materials used in today's world are metals; the demand for their strength generally determines the overall construction weight. In this paper we tested the utilization of superstrong multiwalled boron nitride nanotubes (BNNTs) for making prospective metal matrix composites and present pioneering structural investigations with respect to these newly emerging materials. BNNTs were chosen for such composites because of their excellent mechanical properties, superb thermal and chemical stabilities, extremely high heat resistance and thermal conductivity [1]. In fact, the exciting mechanical properties of individual multiwalled BNNTs have recently been documented using state-of-the-art in situ transmission electron microscopy (TEM) probing techniques [2–4]. These challenging experiments have revealed unmatched mechanical response to a tensile deformation, e.g. ultrahigh tensile strength, more than 30 GPa, and a Young's modulus of up to 1.3 TPa, were documented, as well as outstanding flexibility in bending.

The method of ion implantation has widely been used to modify the surface properties of various materials, and has recently been employed to tailor the properties of nanomaterials. The main objective of these works was to adjust the chemical, mechanical, electronic and optical properties of a given nanomaterial to suit the demands of various technological applications. Typically, carbon nanotubes (CNTs) have grabbed most of the attention. Modifications of CNTs with nitrogen [5,6], sodium [7] and silicon [8] ions have been explored. Only a few studies have considered their non-carbon analogs (TiO_2 and BN nanotubes), and bombardment with light atoms, e.g. N, Ar and He, has been reported [9,10]. To the best of our knowledge, to date there has been no a single report regarding the preparation of BNNT/metal composites using metal ion implantation. We expected that as an outcome of such endeavors multiwalled BN nanotubes covered by a metal layer (and possibly filled by a metal) could be obtained. Such material is envisaged to possess bulk and surface properties attractive for many structural and functional applications. In addition, it is believed that this will become a convenient system for the complete investigation of metal–BN nanotube interfaces and BNNT interactions with a given metallic phase.

Multiwalled BN nanotube samples for metal ion implantation experiments and subsequent analysis were deposited on standard amorphous C-coated copper TEM grids 3 mm in diameter. Pure BNNTs were synthesized via the so-called boron oxide-assisted chemical vapor deposition) method and purified, as described in Refs. [1,2,11]. Diluted suspensions were prepared via BNNT ultrasonication in isopropanol at a ~0.1 μg ml^{-1} concentration; a few drops of these suspensions were then dripped onto the TEM grids. The samples thus

* Corresponding authors; e-mail addresses: shtansky@shs.misis.ru; golberg.dmitri@nims.go.jp

1359-6462/$ - see front matter © 2012 Acta Materialia Inc. Published by Elsevier Ltd. All rights reserved.
http://dx.doi.org/10.1016/j.scriptamat.2012.06.016

obtained were placed in a vacuum chamber in front of the implanter, at 100 mm distance from the ion acceleration zone. Three different cathodes, namely a Ni-based alloy (wt.%: 15–17Cr, 8.5–10W, 3.5–4Mo, <3Fe, 1.2–1.5Ti, 1.2–1.5Al, traces of C, Si, Mn, S, P, Ce and B), pure Ti and Al, were chosen for the initial experiments in order to determine the optimal implantation conditions. Experimental parameters varied in the range 5–30 kV for acceleration voltage (U_{acc}) and 5–30 mA for ion current (I), as listed in Figure 1. In additional tests the values of ion flows and irradiation doses were estimated by measuring the temperature of a Ni plate placed in the sample area, based on the assumption that all the ion flow energy is transformed into thermal energy. The mean Ti and Al ion charges were derived from Ref. [12], whereas for the Ni-based alloy it was calculated according to the content of elements in the alloy.

Implantation-induced structural changes within BNNTs were studied by high-resolution (HR) TEM and Raman spectroscopy. Analysis was performed using a 300 kV JEOL 3100FEF field emission transmission electron microscope equipped with an Omega Filter and an energy-dispersive X-ray (EDX) detector. The samples were also optically characterized using a Jobin Yvon S 3000 Raman spectrometer equipped with a 514.5 nm Ar^+-ion laser line for excitation.

The structural changes in BNNTs depend strongly on both the energy of ions and irradiation doses. By varying the implantation conditions (I and U_{acc}), similar irradiation doses for all samples (within the narrow range of 3–6.3 $\times$ 10^{17} ion cm^{-2} for 10 min) were maintained. Since different regions of BNNTs may receive different doses of irradiation due to a shielding effect, as shown in Figure 1, it was difficult to establish a close correlation between the obtained structures and energetic regimes. Nevertheless, a detailed TEM characterization after irradiation revealed a particular sequence of structural transformations during energetic ion bombardment as described below.

Preliminary studies on high-energy metal ion implantation of a single-crystal Si with various metal targets have revealed that, depending on the type of ions, there is a metal concentration peak at a depth of 50 nm (Ti) and 100 nm (Ni, Al, Cr). These distances are of the same order of magnitude as the BNNT thicknesses utilized. Thus these targets are perfectly suited for BNNT ion-implantation regime optimization.

HRTEM images of typical structures obtained at different ion implantation conditions are shown in Figure 2. Pristine multiwalled BNNTs exhibit specific and highly detectable morphology and structure (Fig. 2a). They are straight, 50–100 nm thick hollow cylindrical structures with the walls consisting of multiple parallel BN shells. In the modified parts of the nanotube samples three major structural types have been detected. TEM images and schematic representation of such structures are demonstrated in Figure 2b–d. Under highly energetic implantation conditions (acceleration voltage ~30 kV, comparatively heavy Ni and Ti atoms) fibers with a uniform amorphous-like structure covered by numerous metallic particles 5–10 nm in size are seen as a result of implantation. In certain cases the traces of surviving BNNT inner channels are clearly seen within such fibers (marked by an arrow). Interestingly, the high-energy irradiation resulted in the localization of metal additives as metallic particles both on the tube surfaces and inside their hollow spaces. As the concentration of implanted metal atoms increases, the probability of Me–Me collision events also increases, resulting in a rapid BNNT saturation with metal and formation of metallic nanoparticles. When a lower acceleration voltage was used (~20 kV), continuous metallic coating was achieved (Fig. 2c). In the latter case the contrast of the structures obtained was much darker compared to the pristine nanotubes due to the increased scattering of electrons on heavy metal atoms compared with light B and N atoms constituting the main tube body. In this case a rather uniform distribution of metal species was documented. Comparatively low-energy metal ion impinging (acceleration voltage ~10 kV, lightweight Al ions) usually generates a large number of defects within tubular shells, resulting in the formation of partially amorphous structures.

As in the low- and medium-energy regimes rather uniform metal–BNNT structures are typically formed, we suppose that these regimes are promising for making ultralight BNNT-reinforced composites using Al-based alloys as the desired cathodes. In accordance with this intention, Al implantation was performed at accelerating voltages of 10–20 kV. Depending on the BNNT position relative to the ion beam, as previously, various structural modifications have been documented. TEM images of Al-implanted BNNTs together with corresponding EDX spectra are presented in Figure 3a–c. In many cases BNNTs with preserved overall structure including the inner channel and multiple shells are still clearly seen in Figure 3a. However, after the implantation, initially straight outer shells of the nanotubes had been partially amorphized due to metal penetration. Numerous dark-contrast areas seen in the TEM images (Fig. 3a) correspond to the nanotube areas experiencing significant stress fields introduced during Al implantation.

A representative TEM image of a BNNT completely modified by Al ions is shown in Figure 3b. The EDX spectra presented in Figure 3 indeed confirm the presence of Al in the fabricated composite. In addition to the peak that corresponds to Al, an oxygen peak is seen in the spectra, implying at least partial Al oxidation. Often the nanotube crystalline structure was essentially preserved (Fig. 3c), while the Al ions formed a continuous layer on its surface and penetrated into the tube inner channels. Such channel filling is evidenced by the dark contrast in TEM images and the presence of an Al peak in the EDX spectra.

In an attempt to shed additional light on the structural changes occurring within BNNTs due to metal ion implantation, Raman spectroscopy was employed. Although resonant conditions are reached within the UV region, Raman spectroscopy with visible excitation is also known to be a powerful tool to analyze BN materials and to obtain insight into their crystallinity [13–16].

Comparative Raman spectra of the nanotube samples before and after Al ion modifications are shown in Figure 3d. Crystalline hexagonal BN materials are characterized by two features in the Raman spectra [13,14]: a low-frequency mode at 52 cm^{-1} that is due to vibrations of the entire BN planes sliding against each other; and a

№	Cathode type/ mean ion charge	Ion implantation			
		Current, mA	U_{acc}, kV	Time, min	Irradiation dose, ion/cm^2×10^{17}
1	Ti/ 2.1	10	30	10	3
2		15	20	10	4.5
3	Ni-based	10	30	10	3.16
4	alloy/ 1.9	10	30	10	3.16
5	Al/ 1.73	10	20	5	1.73
6		10	20	10	3.47
7		10	10	10	3.47

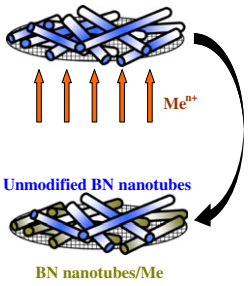

Figure 1. Ion-implantation parameters and schematics of high-energy ion modification of BNNTs during ion implantation.

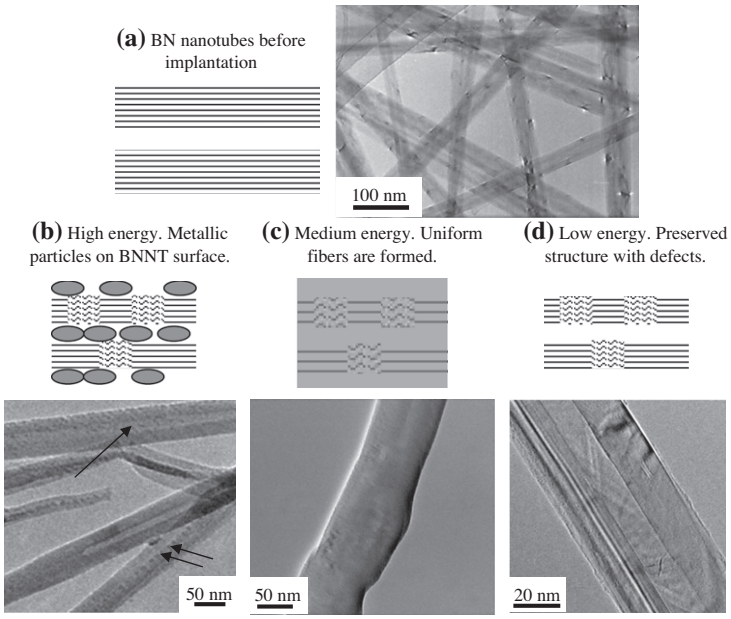

Figure 2. (a)–(c) TEM images and EDX spectra of BNNTs after Al ion implantation at 10 kV and 10 mA. (d) Raman spectra of BNNTs before (black) and after (red) Al ion implantation. (For interpretation of the references to colour in this figure legend, the reader is referred to the web version of this article.)

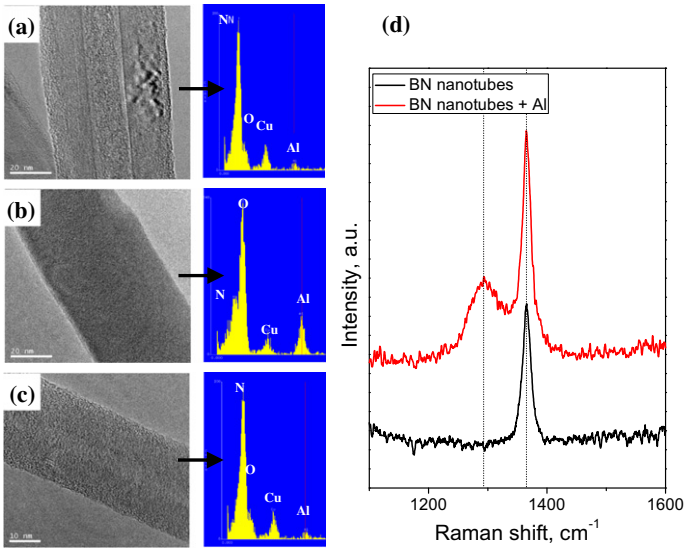

Figure 3. Typical HRTEM images of BNNTs implanted with metal ions at an accelerating voltage of 10–30 kV and an ion current of 10 mA, and corresponding schematic representations of BNNT structures after implantation.

high-frequency mode at 1366 cm^{-1} that corresponds to in-plane vibrations between B and N atoms. This band was observed in both samples tested. The low-frequency mode was not observable due to strong elastic scattering. Additionally, in the Al-modified sample a minor and broad feature around 1293 cm^{-1} appeared in the spectra.

Observation of similar downshifted features has been reported for a row of semiconductors, diamond and graphite [14,15]. According to the spatial correlation model, in an ideal infinite crystal only phonons near the center of the Brillouin zone contribute to the Raman spectrum due to the requirement of momentum conservation between phonons and photons (incident and scattered). In a real crystal, phonons can be confined in space by crystal boundaries and by a wide variety of defects. This gives the phonon momentum uncertainty, allowing phonons with non-zero moments contribute to the Raman spectrum. For most of the crystalline solids the maximum phonon frequency of the highest branch is at the Γ point. However, it has been demonstrated by Nemanich et al. that due to unusual dispersion curves in hexagonal BN an upshift of the 1366 cm^{-1} line takes place before a decrease in the Raman shift due to a reduction in the crystalline size [13,14]. Therefore, only highly disordered hexagonal BN samples are characterized by downshifted high-frequency band.

Based on HRTEM and Raman spectroscopy results we can thus conclude that metal ion implantation leads to the partial amorphization of BNNTs. The presence of both a high-frequency Raman mode at 1366 cm^{-1} and a downshifted broad feature at $\sim$1293 cm^{-1} indicates that the samples are formed by two BN phases: crystalline and amorphous-like. This, together with the above-discussed microscopic data, confirms that the BNNT crystalline structure is at least partially preserved after the implantation process, i.e. a sufficient portion of ordered crystalline hexagonal BN covered by a nanocrystalline or an amorphous phase remains in the ion-implanted samples. Ni et al. [8] studied the structural changes of CNTs produced by Si ion beam irradiation (40 keV, 10^{16}–10^{17} ions cm^{-2}) and reported a two-step process of CNT transformation into solid amorphous C nanowires via semi-solid amorphous C nanowires with hollow structures. Although these stages of transformation were also observed in the present study, our results clearly indicate that the crystalline structure of BNNT partially survived after ion implantation, i.e. the sputtering of metallic targets did not affect the inner structure of the BNNTs but increased metal additive concentration on their surfaces.

To sum up, we investigated the influence of high-energy metal ion implantation on the structure of multi-walled BN nanotubes. Modification of nanotubes was carried out using Ti, Ni-based alloy and Al-implanted ions. Variation of the implantation parameters led to the different metal morphologies/structures—nanosized particles or uniform metal layers—growing on the nanotube surfaces. Different stages of nanotube degradation after ion implantation were detected by TEM. Implantation of comparatively light ions (Al) resulted in less damage in BNNT shells compared to heavier Ti and Ni ions. In order to achieve substantial implantation of BNNT with metals, an irradiation dose of $\sim 10^{17}$ ion cm^{-2} was required. According to EDX spectroscopy measurements, in these conditions metal and/or metal oxide phases appeared at the surface and occasionally in the inner BNNT channels. Raman spectroscopy confirmed that in the regimes of implantation selected as the optimal ones, the BNNT crystalline phase had, at least, partially been preserved. We have thus documented that by changing the ion-implantation parameters it is possible to fabricate BNNT/metal composites with different contents of BNNT crystalline phase and controlled morphologies, structures and volume fractions of metal phase additives. Such novel composite nanomaterials are envisaged to be attractive for many structural and functional applications, in particular as reinforced ultralight Al-based alloys.

This work was supported by the Grant of Russian Federation Ministry for Science and Education (grant no. 11.G34.31.0061). D.G. particularly acknowledges the World Premier International (WPI) Center for Materials Nanoarchitectonics (MANA) of the National Institute for Materials Science (NIMS), Tsukuba, Japan, for using HRTEM facilities and a Mega-Grant Award for the leading scientists tenable at the National University of Science and Technology "MISIS", Moscow, Russia.

[1] D. Golberg, Y. Bando, C.C. Tang, C.Y. Zhi, Adv. Mater. 19 (2007) 2413.
[2] D. Golberg, P.M.F.J. Costa, O. Lourie, M. Mitome, C. Tang, C.Y. Zhi, K. Kurashima, Y. Bando, Nano Lett. 7 (2007) 2146–2151.
[3] D. Golberg, P.M.F.J. Costa, M. Mitome, Y. Bando, In-situ TEM electrical and mechanical probing of individual multi-walled boron nitride nanotubes, in: T. Kijima (Ed.), Inorganic and Metallic Nanotubular Materials: Recent Technologies and Applications, Top. Appl. Phys. 117 (2010) 275–286.
[4] X.L. Wei, M.S. Wang, Y. Bando, D. Golberg, Adv. Mater. 22 (2010) 4895.
[5] F. Xu, M. Minniti, P. Barone, A. Sindona, A. Bonanno, A. Oliva, Carbon 46 (2008) 1489.
[6] F. Xu, M. Minniti, C. Giallombardo, A. Cupolillo, P. Barone, A. Oliva, L. Papagno, Surf. Sci. 601 (2007) 2819.
[7] M. Commisso, A. Bonanno, M. Minniti, P. Barone, P. Riccardi, A. Oliva, L. Papagno, F. Xu, Surf. Sci. 601 (2007) 2832.
[8] Z. Ni, Q. Li, J. Gong, D. Zhu, Z. Zhu, Nucl. Instrum. Methods Phys. Res. B 260 (2007) 542.
[9] A. Ghicov, J.M. Macak, H. Tsuchiya, J. Kunze, V. Haeublein, S. Kleber, P. Schmuki, Chem. Phys. Lett. 419 (2006) 426.
[10] O. Lehtinen, T. Nikitin, A.V. Krasheninnikov, L. Sun, L. Khriachtchev, F. Banhart, T. Terao, D. Golberg, J. Keinonen, Phys. Status Solidi C 7 (2010) 1256.
[11] C.Y. Zhi, Y. Bando, T. Terao, C.C. Tang, H. Kuwahara, D. Golberg, Adv. Funct. Mater. 19 (2009) 1857.
[12] A.G. Nikolaev, E. Oks, G.Y. Yushkov, J. Theor. Phys. 68 (1998) 39.
[13] R.J. Nemanich, S.A. Solin, R.M. Martin, Phys. Rev. B 23 (1981) 6348.
[14] L. Bergman, R.J. Nemanich, Annu. Rev. Mater. Sci. 26 (1996) 551.
[15] J. Hanh, F. Richter, D.R. Zahn, Appl. Phys. Lett. 70 (1997) 958.
[16] R. Arenal, A.C. Ferrari, S. Reich, L. Wirtz, J.-Y. Mevellec, S. Lefrant, A. Rubio, A. Loiseau, Nano Lett. 6 (2006) 1812.